ELSEVIER

Surface Science 411 (1998) 249–262

surface science

CO adsorption and oxidation on bimetallic Pt/Ru(0001) surfaces – a combined STM and TPD/TPR study

F. Buatier de Mongeot [1], M. Scherer [2], B. Gleich, E. Kopatzki [3], R.J. Behm *

Abt. Oberflächenchemie und Katalyse, Univ. Ulm, D-89069 Ulm, Germany

Received 30 November 1997; accepted for publication 13 March 1998

Abstract

The results of a comparative STM and TPD/TPR study on the adsorption and oxidation of CO on pure Ru(0001) and on structurally and compositionally well-defined, bimetallic Pt/Ru(0001) surfaces are presented. The defect structure and local surface composition of the bimetallic substrates, which are produced by epitaxial growth of monolayer Pt islands or by Pt deposition and subsequent surface alloying, are characterized by high-resolution STM images with chemical contrast. TPD and TPR experiments for CO adsorption/oxidation on these surfaces show a distinct lowering of the CO adsorption energy on the bimetallic surfaces with respect to the pure Ru(0001) and Pt(111) surfaces, with the onset of CO desorption already at 230 K. The reduction in adsorption energy is attributed to an electronic modification of the deposit metal due to interaction with the Ru(0001) substrate. The bimetallic surface alloy catalyzes CO oxidation under UHV conditions. The reduced temperature for CO_2 desorption as compared to Pt(111) indicates an even lower barrier than on the latter surface, whereas the pure Ru(0001) surface is inert under these conditions. The results are discussed with respect to the superior CO tolerance of bimetallic PtRu catalysts in low-temperature fuel cells as compared to monometallic Pt catalysts, leading to a mechanistic explanation of that phenomenon distinctly different from previous ideas.

Keywords: Adsorption; Carbon dioxide; Carbon monoxide; Catalytic reaction; Epitaxy; Oxygen; Platinum; Ruthenium; Scanning tunneling microscopy; Structure; Surface alloy; Temperature-programmed desorption

1. Introduction

Bimetallic surfaces have long been known for their catalytic activity and selectivity, which often exceeds that of the individual components [1]. One particular example of this are bimetallic PtRu catalysts, which have found special interest as very CO-tolerant anode catalysts in low-temperature fuel cell applications [2,3], and which may be interesting catalysts also for fuel cell feed gas purification, by selective CO oxidation in a H_2-rich atmosphere [4]. The origin of the increased CO tolerance and activity for CO electrooxidation of PtRu alloy catalysts as compared to monometallic Pt catalysts is still under debate. Both of the components Pt and Ru are known to be very active CO oxidation catalysts as disperse, supported catalysts and under atmospheric pressures (see Ref. [5] and references therein), whereas for

* Corresponding author. Fax: +49 731 5025452; e-mail: juergen.behm@chemie.uni-ulm.de

[1] Present address: Dipartimento di Fisica, Univ. di Genova, V. Dodecanesco 33, I-16146 Genoa, Italy.

[2] Present address: EPFL Lausanne, CH-1015 Lausanne, Switzerland.

[3] Present address: CS GmbH, Fraunhoferstr. 4, D-85737 Ismaning, Germany.

0039-6028/98/$ - see front matter
PII: S0039-6028(98)00286-6

single crystalline Pt(111) and Ru(0001) samples and under UHV conditions, only the former was reported to be active for CO oxidation [6,7]. On the latter, coadsorbed CO_{ad} and O_{ad} are found to desorb unreacted [8–10]. In order to explain the better performance of bimetallic PtRu catalysts, a bifunctional mechanism had been suggested, where the higher affinity of Ru for oxygen nucleation (from H_2O) at low potentials enhances the oxidation of adsorbed CO, which is adsorbed on neighboring Pt sites [11–13]. This mechanism, however, not only ignores the ability of CO to adsorb on Ru, but also assumes that the two components behave similarly as in the respective pure surfaces. Modifications in the chemical behavior of the two components due to interaction with the respective other metal are not included. A better understanding of the reaction process on the bimetallic PtRu surfaces on a microscopic level, however, requires detailed knowledge of the local structure and composition of the bimetallic surfaces and of the local chemical properties of the two metal species in the bimetallic surface. So far, there has been little information available on these aspects.

In this paper, we report first results from a combined scanning tunneling microscopy (STM) and temperature-programmed desorption (TPD) and reaction (TPR) study of adsorbed CO and coadsorbed CO–O adlayers from structurally and morphologically well-defined bimetallic PtRu surfaces, which shed new light on the reaction mechanism and on the physical reason underlying the enhanced CO tolerance of these bimetallic catalysts. The surfaces were prepared by deposition of submonolayer amounts of Pt on a Ru(0001) substrate and subsequent annealing to temperatures below or above the onset of surface alloy formation, respectively. The resulting bimetallic surface was then characterized on an atomic level by high-resolution STM. Depending on the deposition and postannealing conditions, distinctly different surface morphologies can be produced, such as small or larger islands on the Ru(0001) substrate, with ramified or compact shapes, or, for higher annealing temperatures, surface alloys with the Pt atoms dispersed in the topmost Ru substrate layer [14]. We will first present TPD results for CO adsorption on different PtRu bimetallic surfaces and, for comparison, on the pure Ru(0001) surface, together with results of STM measurements on the structure and morphology of the bimetallic surfaces. Here, high-resolution images with chemical contrast allowed a distinction to be made between Pt and Ru surface atoms. In the second part, we describe TPR experiments on these surfaces, testing for CO_2 formation from CO–O adlayers and characterizing the effect of the preadsorbed O_{ad} on CO desorption. The results will demonstrate that: (i) the change to a bimetallic surface layer leads to a drastic reduction in the CO adsorption energy as compared to the pure Pt and Ru substrates; that (ii) there is only a slight difference in the general shape of the CO desorption trace from a Ru(0001) surface partly covered with Pt monolayer islands and from a surface alloy containing equal amounts of Pt atoms (0.4 ML) dispersed in the topmost layer; and that (iii) the bimetallic surface catalyzes CO_2 formation under UHV conditions. The strong reduction in CO adsorption energy on the bimetallic surface is in good agreement with results obtained on heteroepitaxial monolayer films in comparable systems (see Ref. [15] and references therein) and also with theoretical predictions [16–18].

2. Experimental

The TPD/TPR experiments were performed in a UHV system (base pressure $<1\times10^{-10}$ mbar) with standard facilities for surface preparation and characterization, including low-energy electron diffraction (LEED), a single-stage cylindrical mirror analyzer for Auger electron spectroscopy (AES), and a quadrupole mass spectrometer for residual gas analysis and TPD/TPR. To avoid the registration of gas desorption from areas other than the sample surface, the mass spectrometer was surrounded by a cap with a 4 mm aperture positioned in front of the sample. Sample heating was performed by passing a direct current through the two tantalum wires holding the sample. Linear heating ramps of $\beta=2.2$ K s^{-1} (3 K s^{-1} in Figs. 8 and 9) were obtained using a temperature controller. Exposures are given in Langmuir ($1\ \mathrm{L}=1.33\times10^{-6}$ mbar·s), the coverages were

obtained by integration of the desorption traces and normalized to the saturation coverage on pure Ru(0001) of 0.68 ML [19].

The STM experiments were performed in a UHV–STM system equipped with a very rigid pocket size STM and facilities for surface preparation and characterization similar to those in the other system. Further details on the apparatus are given elsewhere [20]. STM images were typically recorded at a bias voltage of 1 V and a tunnel current of 0.6 nA, with atomic resolution images at about 50 mV and 10 nA. STM images are shown in a top-view gray-scale representation, with brighter colors indicating higher surface areas.

The sample was cut to better than 0.5° and polished with alumina powder down to a grain size of 0.05 μm. Further sample cleaning included first cycles of Ar^+ ion sputtering (1 keV, 2.5 μA) and oxidation (10 L O_2 adsorption at 300 K and annealing to 1700 K) [21]. The high temperature of the annealing step was necessary to remove any traces of subsurface oxygen.

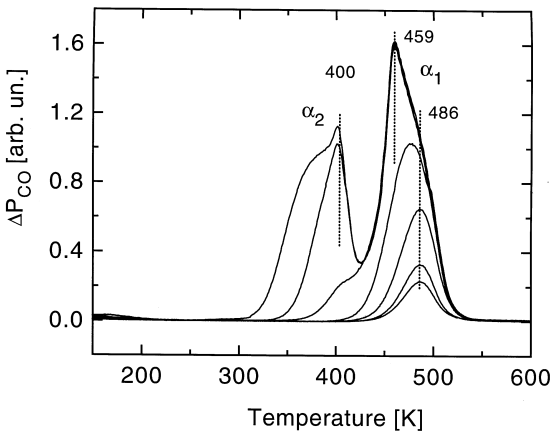

Fig. 1. Set of TD spectra recorded after increasing CO exposures to clean Ru(0001) (0.1 L, 0.2 L, 0.5 L, 1L, 2 L, 3 L and 4 L exposure, $p_{CO}=1\times10^{-8}$ mbar, $\beta=2.2$ K s^{-1}, $T_{exp}=100$ K).

3. Results and discussion

3.1. CO adsorption on Ru(0001) and bimetallic Pt/Ru(0001) surfaces

The clean Ru(0001) surface exhibited an almost perfect topography with large terraces about 100 nm in width separated by monolayer height steps. Atomic resolution STM images showed that the contamination levels were far below the AES detection limit of about 1%.

In a first set of experiments, we checked the CO desorption behavior from these well-ordered and clean, unmodified Ru(0001) surfaces. A set of TPD spectra, obtained after increasing exposures to CO at 100 K (exposure range 0.1–4 L), is presented in Fig. 1. At low coverages, up to about 1.5 L exposure, the spectra exhibit a single desorption peak (α_1-peak). This peak, with a maximum that shifts from 486 K at low coverages to 459 K at saturation, is associated with desorption from the $(\sqrt{3}\times\sqrt{3})$R30°CO structure [19,22]. At higher coverages, for exposures above 1.5 L, a low-temperature shoulder develops, which then grows into a second, lower temperature desorption peak with a maximum at about 400 K (α_2-peak). This latter peak is attributed to desorption from the high-coverage $(2\sqrt{3}\times2\sqrt{3})$R30°CO structure [19,22]. The characteristic spectra are practically identical to those reported in the literature [10,19]. The corresponding activation energies for desorption from the two states had been determined to 38 and 30 kcal mol^{-1}, respectively [19].

Next, we move to bimetallic Pt/Ru(0001) substrates. The first Pt/Ru(0001) surface to be investigated was produced by room-temperature deposition of about 0.4 ML of Pt and subsequent annealing to 800 K. Platinum deposition at room temperature produces a surface covered by small monolayer islands with a characteristic, relaxed dendritic shape, that are homogeneously distributed over the terraces (island density $\sim2\times10^{11}$ cm^{-2}). This is illustrated in the STM image in Fig. 2a. The islands are formed by homogeneous nucleation; the relaxed dendritic shape of the islands indicates that Pt adatom diffusion along the island edges is slow under deposition conditions. Subsequent annealing to 800 K causes these islands to collapse and induces a ripening process, resulting in large, compact islands. Part of the deposited Pt also condenses at the step edges of the Ru(0001) substrate. The modifications during

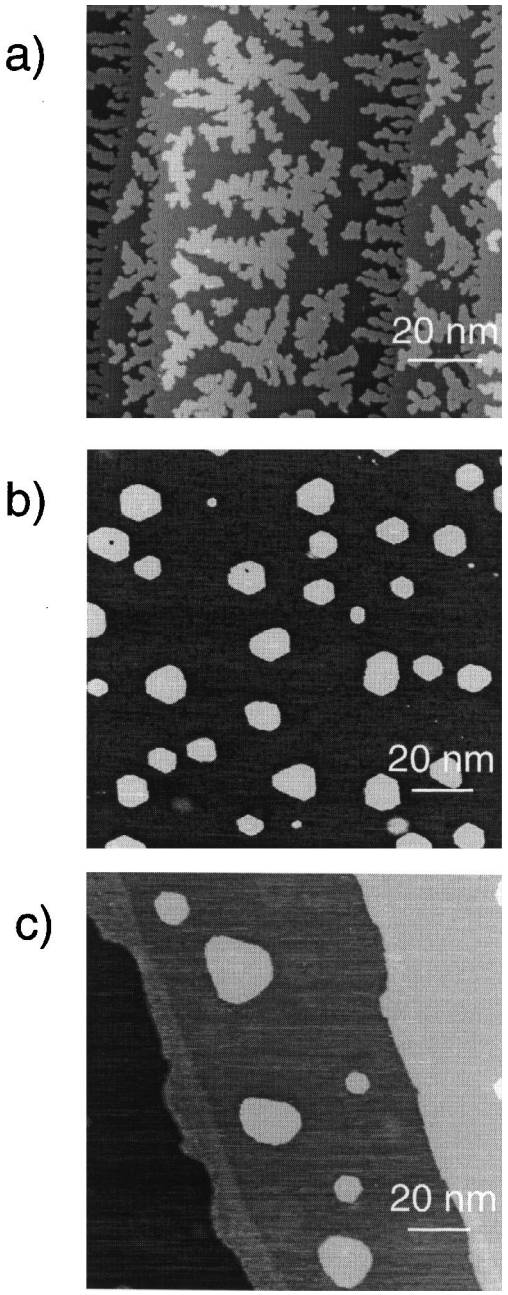

Fig. 2. Set of STM images illustrating the morphology of the submonolayer Pt covered Ru(0001) surfaces after room-temperature Pt deposition and subsequent annealing to temperatures below the onset of (surface) alloy formation. (a) Surface after 0.42 ML Pt deposition at 318 K (117×117 nm); (b) after 0.12 ML Pt deposition at 318 K and subsequent annealing to 736 K (140×150 nm); (c) as (b) but after annealing to 917 K (137×140 nm).

annealing are visible in the images in Fig. 2b and c, recorded on a surface with 0.12 ML Pt after annealing to 736 and 917 K, respectively. From atomic resolution STM measurements, we can rule out any significant amount of surface alloy formation to occur under these conditions. Hence, after room-temperature Pt deposition and subsequent flash annealing to 800 K, the surface is covered by large, compact Pt monolayer islands, with no Pt/Ru intermixing and a small fraction of island edge sites.

CO adsorption on this surface leads to desorption spectra that are markedly different from those obtained on the clean Ru(0001) surface, pointing to a significant change in the CO interaction with the underlying, modified substrate. This is illustrated in the set of TPD spectra (full lines) reproduced in Fig. 3. For comparison, a CO saturation TPD spectrum on pure Ru(0001) (broken line) is included as well. At small coverages (exposure 0.2–1.0 L), desorption occurs in a single peak (γ_1-peak), with a maximum that shifts from 484 K at 0.2 L to 459 K at saturation (≥ 1 L). The desorption temperature of this peak is practically identical to that of the high-temperature α_1-peak on the

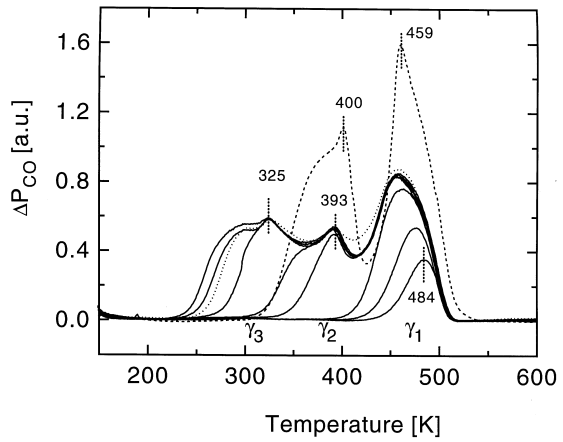

Fig. 3. Set of TD spectra recorded after increasing CO exposures to a Ru(0001) surface covered by Pt monolayer islands (0.4 ML Pt), after room-temperature Pt deposition and subsequent annealing to 800 K (0.2 L, 0.5 L, 1L, 1.5 L, 2 L, 3 L, 4 L and 10 L exposure, $p_{CO} = 1 \times 10^{-8}$ mbar, $\beta = 2.2$ K s^{-1}, $T_{exp} = 100$ K). For comparison, a saturation spectrum (4 L) obtained from the pure Ru(0001) surface is included (broken line).

pure Ru(0001) surface, although there are slight differences in the exact peak shape and in the high-temperature end of the peak. With increasing exposure, a low-temperature shoulder develops into a distinct, separate peak (γ_2-peak), which is filled after exposures of about 1.5–2.0 L. Also, this low-temperature peak very much resembles a scaled-down version of the saturation desorption spectrum on the pure Ru(0001) surface, which, however, was obtained only at higher exposures around 4 L. The underlying reason for the apparent discrepancy in the exposure scales will be discussed in more detail below.

With further increasing exposure, two more peaks develop at even lower temperatures, reflected by a desorption peak with a maximum at around 325 K (γ_3-peak), which saturates after an exposure of about 3 L, and a pronounced low-temperature shoulder developing at even higher exposures (4 and 10 L). Under the present conditions, for adsorption at 100 K, saturation is reached after a CO exposure of about 10 L. The CO saturation coverage on this bimetallic surface is about 0.6 ML, i.e., about 10–15% less than on the unmodified pure Ru(0001) surface.

The desorption spectra contain contributions from two different surface areas, from the pure Ru(0001) substrate and from the monolayer Pt-covered surface. To test whether there is any significant contribution from the island edges, as observed for CO adsorption on Au covered Pd(111) [23], we also recorded a spectrum on this Pt/Ru(0001) surface before the 800 K annealing step, where, because of the ramified shape, the fraction of island edges was higher than after annealing (dotted line, 4 L exposure). Although, in its general shape, the spectrum closely resembles the other 4 L spectrum obtained after 800 K annealing, we notice slight changes. First, the onset of desorption is shifted to slightly higher temperatures, and second, the minimum between the two peaks at 393 and 459 K is less pronounced, reflecting additional CO desorption in that temperature range. These effects shall be investigated in more detail in future. So far it appears, however, that edge sites have a much smaller effect on the CO desorption behavior on this surface as compared to pure Pt surfaces. For stepped Pt(111) surfaces, CO bonding at steps was found to be 0.7 eV more stable than on terraces [24], giving rise to a well-defined desorption state around 500 K [25]. Finally, it should be noted that a control experiment with 4 L exposure at the end of the sequence showed no differences as compared to the initial 4 L spectrum, indicating that the surface was not altered during the TPD experiments.

This desorption series leads us to three main results:

(1) On the bimetallic Pt/Ru(0001) surface at 0.4 ML, Pt CO desorption starts at much lower temperatures than on the pure Ru(0001) or Pt(111) surfaces. For saturation exposure, it begins at about 230 K instead of 300 K as on Ru(0001) and on Pt(111) [26,27].
(2) The population and saturation of the higher temperature states occur at lower exposures than on pure Ru(0001).
(3) The high-temperature states have their peak maximum at about the same temperature as that observed for desorption from a pure Ru(0001) surface.

The earlier onset of CO desorption from this bimetallic surface indicates a reduced adsorption energy for CO on the monolayer Pt covered surface areas (at saturation). Using a preexponential of $v = 10^{13}\ s^{-1}$, and assuming first-order desorption kinetics one can estimate a reduction by about 0.25 eV for saturation coverage as compared to Pt(111). Similar effects have been reported recently for other metal surfaces covered by a monolayer platinum metal films [15] and also for Pt alloy surfaces covered by a Pt monolayer, such as, for example, Pt-rich PtNi alloys [28]. The change in CO adsorption energy was found to be correlated with shifts in the surface core levels of the overlayer metal as compared to their position for the pure metal [15]. For example, for the comparable system Pd/Ru(0001), a downshift in CO desorption temperature by 120 K was reported [29], equivalent to a strong reduction in CO adsorption energy. These authors found the Pd(3d) peak to be shifted by 0.3 eV compared to its binding energy in Pd(100). These changes were attributed to a modification of the electronic structure of the deposit metal as compared to the bulk metal due to interaction with the metal substrate.

Calculations show that these effects are correlated with a depopulation of the d-band at the surface [30,31]. The general trend in these systems suggests that upon formation of the Pt–Ru metallic bond, the population of the Pt d-band decreases and that the center of the d-band shifts to lower energies [16–18]. These effects in turn affect the ability for surface–adsorbate charge donation and therefore reduce the strength of the Pt–CO bond [16,17]. Geometrical effects, caused by the compression of the Pt in the pseudomorphic adlayer islands (Pt–Pt spacing 2.704 Å as compared to the Pt–Pt bulk spacing of 2.774 Å) were proposed to play a major role for this change in the electronic structure of the metal film and the resulting change in metal–CO interaction (J.K. Nørskov, pers. commun. [32]).

Since both pure Ru- and Pt-covered areas are present on this surface, the two higher temperature states that appear at similar temperatures as on the Ru(0001) surface are tentatively associated with desorption from the pure Ru surface areas. The slight change in shape and in particular the shift of the high-temperature end to a lower temperature, by about 12 K, point to a slightly accelerated desorption process. This can be explained by the additional pathway for CO desorption from partly Pt-covered surfaces. In a simple model calculation, the increase in desorption rate caused by parallel desorption from Pt islands, where CO is less strongly bound, and from Ru(0001) areas, in combination with rapid mass transport of adsorbed CO between these areas, can be calculated to about 10–15 K, which is identical to the experimental findings. The faster population of the Ru(0001) related states on the bimetallic surface as compared to adsorption on the pure Ru(0001) substrate equally points to mass transport processes in the lower coverage regimes, with CO molecules impinging on the Pt-covered areas diffusing to the higher adsorption energy Ru(0001) areas. From the TPD data, we cannot decide whether the redistribution of CO molecules occurs upon adsorption or only at the higher temperature during the desorption experiments. For CO adsorption on the stepped Pt(111) system, recent data indicate that adsorbate diffusion to the more strongly adsorbing step sites already occurs quantitatively at 125 K, immediately following adsorption [33], so that similar conclusions should hold also in the present case.

More information on this aspect can be obtained from high-resolution STM images. After CO adsorption (1.2 L) on Ru(0001) at 318 K, we find a well-ordered structure in high-resolution STM images (see Fig. 4a). From the distance of ~4.1 Å between neighboring maxima and from the orientation of the close packed rows of maxima, which

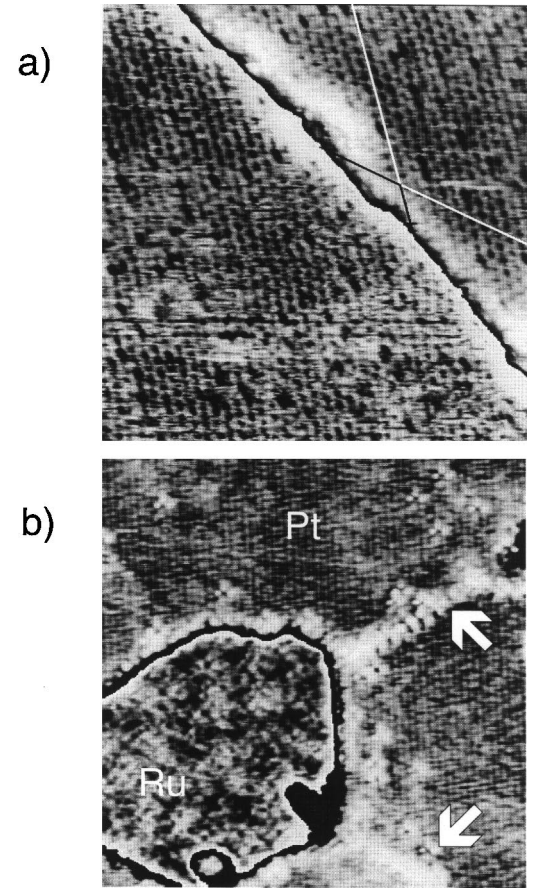

Fig. 4. High-resolution STM images of the CO-covered pure Ru(0001) and partly Pt-covered bimetallic Pt/Ru(0001) surfaces. (a) $(\sqrt{3}\times\sqrt{3})$R30°CO structure on the Ru(0001) substrate obtained after exposure to 1.2 L CO at 300 K (15×15 nm); (b) Ru(0001) surface partly covered with monolayer Pt islands after exposure to 300 L, showing a $(\sqrt{3}\times\sqrt{3})$-R30°CO structure on the Ru(0001) area and no resolvable structure on the Pt monolayer covered areas, except for the decoration of a domain boundary in the Pt layer (see white arrows) (14×15 nm).

is 30° rotated with respect to the close packed rows of the Ru(0001) atomic lattice, we can identify this structure as a $(\sqrt{3}\times\sqrt{3})R30°$ phase, which corresponds to the well-known structure of a 0.33 ML CO adlayer on Ru(0001) [19]. After exposing a surface partly covered by Pt monolayer islands to CO (saturation exposure) the situation is different. In high-resolution STM images of such surfaces, we find a partly ordered $(\sqrt{3}\times\sqrt{3})R30°$ adlayer structure on the flat Ru terraces between the monolayer Pt islands, but only the atomic Pt structure on the Pt monolayer islands. The defects in the $(\sqrt{3}\times\sqrt{3})R30°$ structure on the Ru areas are introduced as the CO coverage exceeds 0.33 ML [19]. On top of the monolayer Pt islands, adsorbed CO is found only at the domain boundaries (white arrows) between fcc and hcp stacked Pt islands and at defects [14] that apparently stabilize CO bonding in a $(\sqrt{3}\times\sqrt{3})R30°$ structure (see Fig. 4b). Hence, after adsorption at room temperature, there is a significant difference in the CO adlayer coverage between the two surface areas, leading to a stable, oversaturated $(\sqrt{3}\times\sqrt{3})R30°$ phase on the Ru(0001) terraces, but not on the monolayer Pt islands. These results confirm (1) that CO diffusion to the more strongly adsorbing Ru patches already takes place at adsorption, in this case at 318 K, and (2) our TPD observation of a significant reduction in adsorption energy for CO on a pseudomorphic Pt monolayer film on Ru(0001) as compared to Pt(111). On the latter surface, an ordered $c(2\times4)$ phase would be expected under similar conditions [34]. It should be noted that the preferential CO adsorption on Ru areas is in contrast with the assumptions made for the proposed bifunctional mechanism for CO oxidation on PtRu alloy, where preferential CO adsorption on Pt sites was anticipated [11,12].

For a more direct comparison with bimetallic PtRu alloy surfaces, the annealing temperature was increased stepwise. After annealing at 1250 K, STM images show that the Pt monolayer islands are dissolved. However, AES spectra indicate only slight losses in the Pt intensity. Clear proof for surface alloy formation with both components in the topmost layer comes from high-resolution STM images with chemical contrast. As shown in the image in Fig. 5, two atomic species are clearly resolved. The "dark" atoms contribute about 30% of the surface atoms. By comparison with the known Pt coverage and with AES, these can be identified as Pt atoms, which means that about 0.12 ML of the initial Pt deposit have dissolved into the bulk. The distribution of the Pt atoms in the surface seems to be roughly random. A quantitative evaluation of several images yields only a slightly higher density of small aggregates of Pt atoms in the surface layer than expected from random deposition. It should be noted that the apparently lower position of the "dark" Pt atoms ($\Delta z\approx0.4$ Å) most likely results from differences in their electronic properties rather than reflecting a geometric effect. This interpretation is supported by the net charge transfer from Pt to Ru occurring upon formation of the metal–metal bond [15].

CO TPD spectra recorded from this surface are presented in Fig. 6. Overall, the spectra resemble those obtained from the 800 K annealed surface (Fig. 3), although they have a less pronounced peak structure. Up to about 1.5 L, desorption occurs in a single peak (ρ_1-peak), which is again attributed to desorption from (local) Ru areas, as

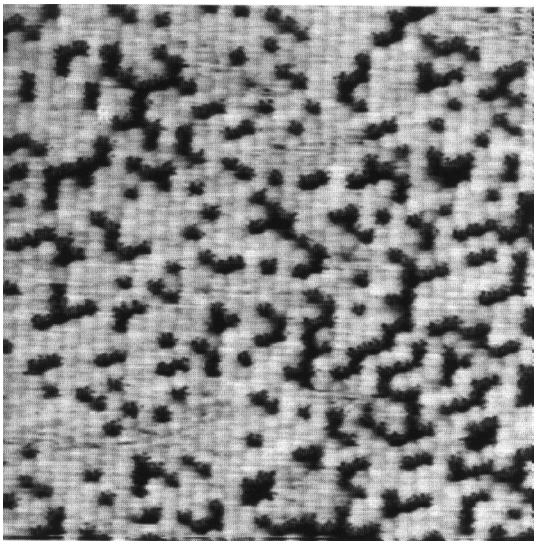

Fig. 5. High-resolution STM image of a PtRu surface alloy formed by deposition of 0.42 ML Pt at 310 K and subsequent annealing to 1200 K (8.5×10.2 nm, $U_t=9$ mV, $I_t=56$ nA). The Pt atoms (31% surface concentration) are imaged as lower-lying "darker" atoms due to electronic effects.

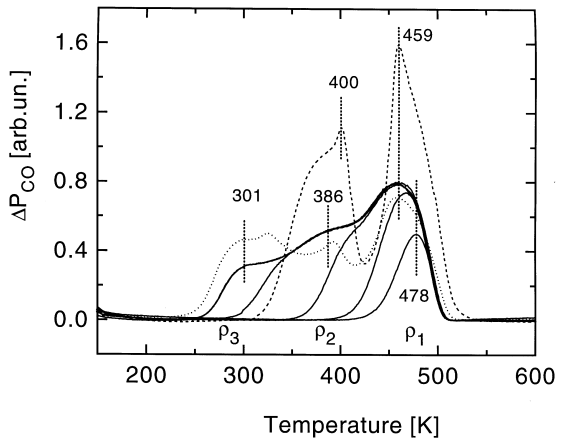

Fig. 6. Set of TD spectra recorded after increasing CO exposures to a bimetallic PtRu(0001) surface alloy prepared by room-temperaure deposition of 0.4 ML Pt and subsequent annealing to 1250 K (0.5 L, 1 L, 2 L, 3 L, 4 L and 10 L exposure, $p_{CO}=1\times10^{-8}$ mbar, $\beta=2.2$ K s^{-1}, $T_{exp}=100$ K). For comparison, saturation spectra obtained from the pure Ru(0001) surface (4 L) and from the 0.4 Pt monolayer island covered surface (10 L) are included as a broken and dotted line, respectively.

the peak position coincides with the Ru(0001) α_1 desorption peak. For exposures above 1.5 L, a low-temperature shoulder grows and expands steadily to lower temperatures with increasing exposures. At saturation, desorption starts at about 250 K, which is at a slightly higher temperature than for desorption from Pt monolayer covered surface areas. Because of the rather smooth structure of the spectra with only slight humps at 301 K [ρ_2-peak] and 386 K [ρ_3-peak], a further assignment of distinct adsorption states is hardly possible, unless other spectroscopic data are available. Apparently, CO–CO repulsions and modifications in the interaction with the metal substrate imposed by the presence of the Pt atoms in the surface ("ligand effects") together lead to a continuous decrease in adsorption energy with coverage as soon as the high-temperature state is filled. Qualitatively, the presence of Pt atoms in the surface alloy has a similar effect on adsorbed CO as a pseudomorphic Pt cover layer: it significantly reduces the CO adsorption energy. Also this result agrees excellently with theoretical predictions. Ruban et al. found that the energy shift in the center of the d-band is almost identical for a pseudomorphic Pt overlayer on Ru(0001) and for a Pt impurity in the Ru(0001) surface [18]. Following the line of arguments described above, that would lead to a similar reduction in CO adsorption energy for CO adsorption on a Pt overlayer or on a Pt impurity site, in a PtRu surface alloy.

3.2. CO–O coadsorption on Ru(0001) and bimetallic Pt/Ru(0001) surfaces

In the second part, we present results for the competing CO desorption and oxidation from a CO–O coadsorbate layer, which is relevant for understanding the catalytic properties of these surfaces. Similar to the procedure for CO adsorption, we first reproduce TPD and TPR data obtained from coadsorbed CO–O adlayers on the unmodified Ru(0001) surface for comparison with previous results [8–10,35–38]. The spectra presented in Fig. 7, which were recorded from surfaces with increasing oxygen precoverage exposure at 100 K and subsequent saturation with 4 L CO,

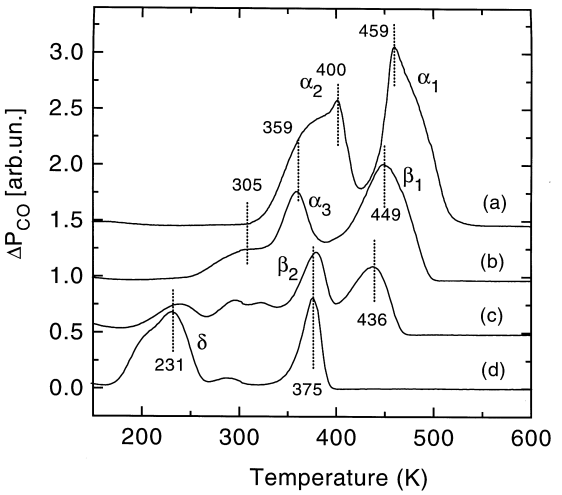

Fig. 7. Set of CO TPD spectra recorded after CO adsorption on a O-precovered Ru(0001) surface with increasing O precoverages. (a) 4 L CO on the clean surface; (b) 1 L O_2 preexposure at 100 K, subsequent exposure to 4 L CO; (c) additional exposure of 1 L O_2 and 4 L CO on the surface obtained after spectrum b; (d) additional exposure of 5 L O_2 and 4 L CO on the surface obtained after spectrum (c) ($p_{CO}=5\times10^{-8}$ mbar, $\beta=2.2$ K s^{-1}, $T_{exp}=100$ K).

reproduce the detailed TPD data by Kostov et al. in all essential features [10]. We therefore give a brief account only at this place, concentrating on those aspects that are relevant for the present study.

Starting with desorption from the clean surface (spectrum a, 4 L CO) the following spectrum (b) was recorded after 1 L O_2 preexposure at 100 K and subsequent exposure to 4 L CO. The O_2 preexposure is sufficient to produce a (2×2) O adlayer with $\theta_O=0.25$. Similar to desorption from a pure CO adlayer, the resulting desorption spectrum shows two peaks that, however, are shifted to lower temperatures. These correspond to the β_1-peak (T_{max} = around 440 K) and the α_3-peak (T_{max} = around 360 K) in Ref. [10]. The larger temperature difference between these two peaks supports the interpretation in Ref. [10] that these states do not refer to desorption from CO islands, but result from CO adsorbed into the (2×2)O matrix. Furthermore, we find an additional low-temperature shoulder centered just above room temperature. The total CO coverage is reduced to about 0.52 ML, equivalent to about two CO molecules per (2×2) unit cell. The low-temperature shift of the maxima reflects repulsive interactions between O_{ad} and CO_{ad}. Due to these repulsions, the onset of CO desorption at saturation is moved by 50 K to lower temperatures, to about 250 K. The hump at room temperature may be attributed to CO adsorbed at defects in the adlayer. No CO_2 desorption was observed.

In the next experiment, the resulting surface was again exposed first to 1 L O_2 and then to 4 L CO. It is important to note that the oxygen left from the adsorption in the last experiment is still present on the surface before this second coadsorption experiment. (Since O does not desorb at temperatures below 600 K, the successive exposure to O_2 leads to an accumulation of O_{ad} on the surface.) Following earlier studies, after 2 L O_2 exposure, the surface will be covered by coexisting (2×2) and (2×1) areas [39]. The CO TPD spectrum resulting from this surface again differs significantly from the previous spectra. The high-temperature peak continued to lose intensity and to shift to lower temperatures. Instead of the low-temperature Ru(0001) related peak, we now find a distinct peak at 375 K (β_2-peak in Ref. [10]), and a number of smaller peaks with maxima at 240, 295 and 320 K. The former peak was associated with CO adsorption into a well-ordered O matrix, the latter with CO adsorbed into a disordered high coverage O phase [10]. Due to the interaction with coadsorbed O_{ad}, the onset of CO desorption is shifted by another 50 K to lower temperatures, to about 200 K. At saturation, a CO coverage of 0.37 ML is obtained on this surface.

Finally, for another 5 L O_2/4 L CO exposure, the high-temperature CO-state is completely depleted. Instead, the spectrum now exhibits two major adsorption states, the β_2-peak at 375 K already observed in the previous spectrum and a new low-temperature peak centered at 231 K (δ-peak in Ref. [10]). This latter state presumably developed from the small low-temperature hump at 240 K mentioned for the last experiment. Furthermore, there is a small peak at 300 K, reminiscent of the peaks at 295 and 320 K in the last experiment. The total coverage in this spectra is now 0.27 ML, less than half of the saturation coverage on the clean surface, and the onset of desorption occurs at about 170 K.

From the total exposure of 7 L O_2, one can estimate that prior to CO adsorption the surface was largely covered by a $p(2\times1)$ O adlayer with $\theta_O=0.5$. The coverage of 0.27 ML CO, however, is inconsistent with a model with 1 CO molecule per (2×1) unit cell. In fact, it was proven in a recent LEED I/V analysis that at least part of the initial (2×1)O adlayer rearranges into a honeycomb structure upon CO coadsorption [40]. In this oxygen matrix, all of the adsorbed CO molecules are in the direct neighborhood of an O adatom, and hence all of these molecules undergo a distinct CO–O interaction, which, following the present results, is strongly repulsive. From the absence of any CO_2 desorption, CO oxidation can be excluded.

Following these experiments, we performed similar TPR measurements on the PtRu alloy surface produced as described above (0.45 ML Pt deposited, annealed to 1300 K). The most important result with respect to the catalytic activity of these surfaces is the fact that part of the adsorbed CO now reacts with coadsorbed O to form CO_2. The

CO and CO_2 desorption spectra obtained after 1 L and 10 L O_2 preexposure, respectively, are reproduced in Figs. 8 and 9.

For comparison with subsequent spectra from the CO–O adlayer, we first recorded CO and CO_2 spectra from the CO-saturated surface (10 L CO exposure), with no coadsorbed oxygen. Furthermore, O_2 desorption spectra were recorded also in all experiments. The CO desorption spectrum (spectrum 1 in Fig. 8a) shows the normal desorption behavior for a CO-saturated surface, resembling that in Fig. 6. Small deviations are attributed to the slightly higher Pt concentration. No CO_2 desorption is detected (spectrum 1, Fig. 8b). After exposure first to 1 L O_2 and then to 4 L CO, we observe CO_2 desorption in a distinct peak (χ_1-peak) between 200 and 350 K (T_{max} about 275 K, spectrum 2 in Fig. 8b), followed by a low-intensity regime (χ_2 desorption regime) up to 473 K. Clearly, CO oxidation is now a process that competes with CO desorption. Based on the CO_2 intensity in the TPR spectrum, about 20% of the adsorbed CO, equivalent to about 0.1 ML, reacts to CO_2. CO desorption occurs in a wide double peak between 250 and 473 K (φ_1-peak and φ_4-peak) (spectrum 2 in Fig. 8a). Comparison with CO desorption from a pure CO adlayer shows distinct changes in the desorption trace. First of all, the amount of CO desorption is reduced to 0.29 ML, 53% of the original value of 0.55 ML.

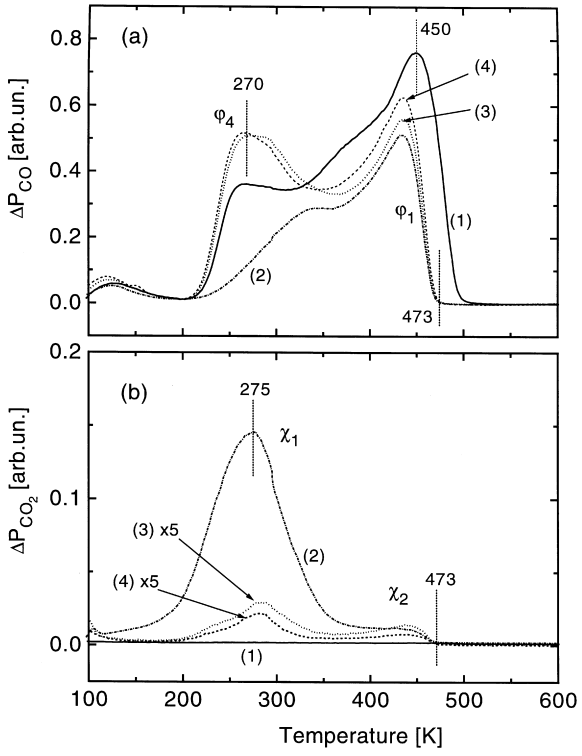

Fig. 8. Set of TPD/TPR spectra [(a) amu 28, CO and (b) amu 44, CO_2] recorded after CO adsorption on an O-precovered bimetallic Pt/Ru(0001) surface alloy (0.45 ML Pt, annealed to 1300 K). Reexposure for a new spectrum took place on the surface obtained after the last desorption run. From top to bottom: (1) 4 L CO on the clean surface; (2) 1 L O_2 preexposure at 100 K followed by 4 L CO (CO_2 signal × 5); (3) additional exposure to 4 L CO; (4) additional exposure to 4 L CO (CO_2 signal × 5) ($p_{CO} = 1 \times 10^{-8}$ mbar, $\beta = 3$ K s^{-1}).

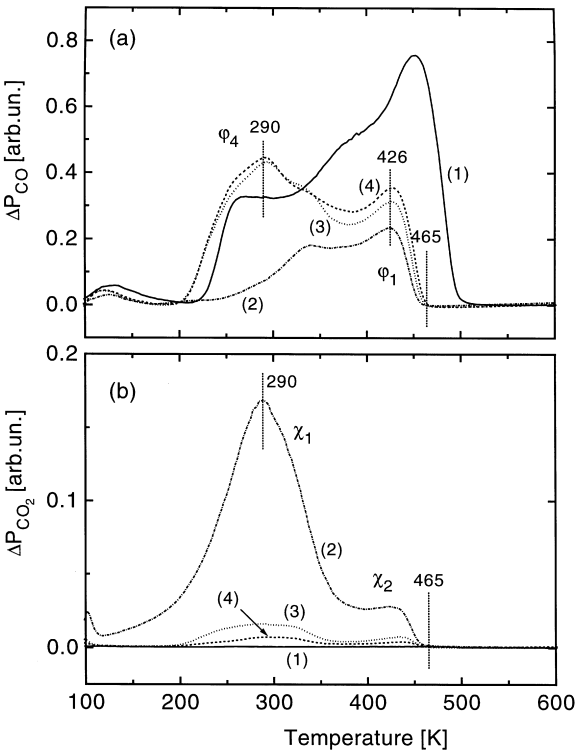

Fig. 9. Set of TPD/TPR spectra [(a): amu 28, CO and (b): amu 44, CO_2] recorded after CO adsorption on an O-precovered bimetallic Pt/Ru(0001) surface alloy (0.45 ML Pt, annealed to 1300 K). Reexposure for a new spectrum took place on the surface obtained after the last desorption run. From top to bottom: (1) 4 L CO on the clean surface; (2) 10 L O_2 preexposure at 100 K followed by 4 L CO (CO_2 signal × 5); (3) additional exposure to 4 L CO; (4) additional exposure to 4 L CO (CO_2 signal × 5) ($p_{CO} = 1 \times 10^{-8}$ mbar, $\beta = 3$ K s^{-1}).

This reduction in CO desorption results from two effects: from a decrease in CO uptake on the O_{ad} precovered surface, similar to the findings for the unmodified Ru(0001) surface, and from a partial reaction to CO_2. Since the latter is determined to be about 20% of the total CO coverage, O_{ad} induces a reduction in CO uptake by about 0.16 ML. The loss in CO intensity occurs over the entire desorption range. It is specifically pronounced for the low-temperature peak at 270 K (φ_4-peak), which is essentially depleted. Furthermore, the high-temperature desorption peak (φ_1-peak) is shifted by 10 K to lower temperatures, from 450 K to 440 K. Together with the downshift in peak temperature, also the high-temperature end of the desorption is shifted by 15 K to 473 K. Both CO and CO_2 desorption end at exactly the same temperature, indicating that the end of CO oxidation is limited by CO supply. The O_{ad}-induced shift to lower temperatures for the desorption peak and for the end of the desorption trace reproduces the trends observed on the pure Ru(0001) substrate, although the effects are more pronounced on the PtRu surface alloy. It should be noted that during this run, also a small amount of O_2 desorption was observed (about 0.001 ML).

Similar to the procedure on Ru(0001), we again saturated the resulting surface with CO (4 L exposure) and recorded the desorption spectra (spectrum 3 in Fig. 8a and b). The CO TPD spectrum differs significantly from both of the previous spectra. It is significantly larger than the last spectrum, but still somewhat smaller than that obtained for desorption from a purely CO saturated surface (spectrum 1). Interestingly, the low-temperature φ_4-peak at 270 K exceeds that of the first spectrum, indicative of an O_{ad}-induced state at this temperature. The high-temperature φ_1-peak only increases in intensity with respect to spectrum 2. The peak position and its high-temperature end do not shift in temperature. These results provide clear evidence that part of the initial O_{ad} is still on the surface. Hence, CO oxidation in the previous desorption run was not O_{ad}-limited. The tendency for CO oxidation is strongly reduced. The CO_2 desorption intensity is only about 3% of that produced in the last run. Whereas the position and shape of the main peak (χ_1-peak) did not change, the low-intensity χ_2 regime is more pronounced relative to the main peak, growing to a distinct maximum at 438 K. This much lower probability for CO oxidation, despite significant amounts of O_{ad} on the surface, indicates that the remaining O_{ad} is much less reactive with respect to CO oxidation. Most of the reactive O_{ad} available must have already been removed in the first heating cycle. These conclusions are supported by a second similar experiment (spectrum 4), where even less CO_2 formation is observed, whereas the CO desorption spectrum hardly changes. As expected from the small amount of CO_2 formation, the CO TPD spectrum increases only by a small amount during this experiment. No O_2 desorption was observed during these latter desorption runs.

These results point to a reaction mechanism where two different kinds of oxygen exist on the surface, one that is largely inert with respect to CO oxidation (under UHV conditions) and one that is accessible for this reaction. From the present data, it is not possible to determine the origin of these states. It may be due to repulsive interactions between closely spaced, neighboring O adatoms that modify the energetics of these adatoms and thereby enhance the reaction probability, or, more likely, it may be caused by different binding configurations, i.e., by different metal ensembles serving as adsorption sites for the O adatom. From the observation of a small amount of O_2 desorption at low temperatures, one may also speculate that a molecular oxygen species is involved in this reaction. However, since most of the O_2 desorption takes place at temperatures between 100 and 200 K, while on the other side, CO oxidation takes part mostly at temperatures above 200 K, we consider this possibility to be unlikely. Further experiments are planned to investigate this in more detail.

To gain more information on the role of the coadsorbed oxygen, we performed a second, similar set of experiments, on a surface alloy prepared as in the previous experiments, but increasing the O_2 preexposure to 10 L. The resulting TPD and TPR spectra are reproduced in Fig. 9. Again, we first recorded CO and CO_2 desorption spectra for control prior to O_2 exposure (spectra 1). The spectra underline the close similarity between the

alloy surfaces in the two experiments. The first set of desorption spectra recorded from the mixed CO–O adlayer (spectra 2) leads to the following results: first of all, we again find an appreciable amount of CO oxidation, with a similar CO_2 desorption peak as observed after 1 L O_2 preexposure. Also, the peak intensity is comparable with that in the latter experiment. Carbon dioxide formation starts again at 150 K (not including the low intensity tail starting at the lowest temperatures), with the peak maximum shifted to slightly higher temperatures, to around 290 K. This shift must result from the higher O_{ad} precoverage. The transition to the high-temperature χ_2 desorption regime, which is observed also for this higher O_2 preexposure, occurs at about 360 K. This desorption feature, however, is much narrower than in the previous case. Carbon dioxide desorption ceases at about 465 K. Also, in this case, it coincides with the completion of CO desorption. Hence, CO oxidation in this temperature regime is again limited by CO supply.

The shape of the CO desorption spectrum recorded simultaneously (spectrum 2) resembles that obtained after 1 L O_2 preexposure. The intensity loss, however, is significantly stronger than in the latter case. The CO desorption signal is reduced to about 0.14 ML. Accounting for the oxidized CO, the total CO coverage must have been around 0.24 ML. A more detailed inspection reveals also that the downshift in temperature of the main peak is slightly stronger. The peak maximum is at 426 K and ends at about 465 K. The low-temperature state at around 295 K (see below) is again completely absent. As before, we find a small amount of O_2 desorption (0.001 ML), most of which occurs in a wide peak between 100 and 200 K.

Reproducing the experimental sequence after 1 L O_2 preexposure, the resulting surface was subsequently saturated with CO to characterize the state of that surface (spectra 3 and 4). The results are very similar to those in previous experiments. Again, appreciable amounts of O_{ad} must have remained after the first desorption run, as evidenced from the CO desorption trace. This time, the high-temperature χ_2 desorption regime peak remains at a much lower intensity than in spectrum 1. The CO_2 desorption traces are essentially identical to those in Fig. 8, although the intensity difference between the first and second run after O_2 dosing (spectra 2 and 3) is not quite as strong as before. Nevertheless, also under these conditions, there must have been two different oxygen species with a strongly different reactivity for CO oxidation.

In total, the spectra obtained from a mixed CO–O adlayer show clearly that on the bimetallic surfaces, CO oxidation is not inhibited under UHV conditions as on pure Ru(0001) substrates, but occurs as a minority reaction, in addition to the still-dominant CO desorption. The maximum of the CO_2 desorption χ_1-peak (275–290 K) is well below that for reactive CO_2 desorption on Pt(111), which was reported to be around 330 K [26]. This suggests that the barrier for CO oxidation is lower on the bimetallic surface than on the unmodified Pt surfaces.

4. Conclusions and mechanistic consequences

These experiments lead to the following conclusions for CO adsorption and oxidation behavior on bimetallic Pt/Ru(0001) surfaces:

(1) The adsorption energy of CO on a Pt monolayer island covered Ru(0001) surface or on a PtRu surface alloy is significantly lower than that on either of the two pure surfaces. For 0.4 ML Pt, the onset of desorption is shifted to about 230 K on the Pt monolayer island covered Ru(0001) surface and to 250 K on the surface alloy. Therefrom, a reduction of the adsorption energy at saturation by about 0.25 eV is estimated as compared to adsorption on the pure Ru(0001) and Pt(111) surfaces. A similar reduction in CO adsorption energy was found for a large number of other platinum metal-on-metal systems [15] and also for Pt alloys covered by a Pt overlayer [28]. This was attributed to an electronic modification of the deposit metal, due to interaction with the chemically different substrate [15]. The electronic modifications are reflected also by shifts in the binding energies of the deposit core levels. This explanation was confirmed

by recent calculations [16–18]. They found (1) shifts in the center of the d-band of the bimetallic surface as compared to the bulk deposit metal and (2) a direct correlation between the CO adsorption energy and the shift in d-band center. For Pt/Ru(0001), these calculations showed furthermore that there was almost no difference in d-band position between a Pt overlayer and a PtRu surface alloy. Part of the electronic modifications are caused by geometric strain effects, namely the expansion or contraction of the metal overlayer due to the misfit to the underlying substrate [15,32]. In fact, calculations showed this strain contribution to be often the dominant effect (J.K. Nørskov, pers. commun.). Strain effects should be most pronounced for systems with a large misfit and a pseudomorphic adlayer, as is the case in the present system [Pt–Pt bulk distance: 2.774 Å; Pt–Pt distance in the pseudomorphic Pt/Ru(0001) monolayer islands: 2.704 Å]. Hence, a similar, geometry-based modification of the Pt electronic properties is suggested also for the present system, both for the Pt monolayer covered surface areas and for the Pt/Ru(0001) surface alloy. The downshift in the center of the d-band expected for a compressed Pt overlayer fits well with the observed reduction in CO adsorption energy on the Pt monolayer island covered Ru(0001) surface as compared to bulk Pt(111). A modification of the Ru atoms, in particular in the surface alloy, is possible, but could not be tested in our experiments.

(2) Different from Ru(0001), but similar to Pt(111), the bimetallic Pt/Ru(0001) surface is not inert with respect to CO oxidation under UHV conditions. Upon heating a bimetallic Pt/Ru(0001) surface with coadsorbed O_{ad} and CO_{ad}, an appreciable amount of CO_2 formation is observed, in addition to the dominant CO desorption. In fact, the reaction barrier for CO oxidation on the bimetallic Pt/Ru(0001) surface alloy is lower than on pure Pt(111), as evidenced by the reduction of the CO_2 desorption temperature from a peak maximum of about 330 to about 280 K. The higher reactivity compared with the pure Ru(0001) substrate can be easily explained by assuming an on average lower binding energy of oxygen to the alloy surface. The very high O adsorption energy on the pure Ru(0001) surface at the lower coverages accessible under UHV conditions was indeed held responsible for the inhibition of CO oxidation under UHV conditions [13,37,38], whereas at ambient pressures, a weakly bound high coverage state can be populated that is highly active towards CO oxidation [7]. A "more Pt-like" behavior of the bimetallic surface is reflected also by the observation of a small amount of O_2 desorption at low temperatures, indicative of a stable molecular adspecies on that surface. The reduction in activation barrier below that observed on the pure Pt(111) surface, however, requires a more complex explanation, where the electronic changes in the metal species have to be included as well. For a clear picture of the reaction mechanism, it is also necessary to obtain information on the steady-state O coverage during reaction, since this strongly affects the (competing) CO desorption behavior.

(3) The reaction experiments with preadsorbed oxygen revealed two different O_{ad} species on the bimetallic surface alloy species, one being practically inert with respect to CO oxidation and the other one being reactive under UHV conditions. The physical origin of these differences, e.g., compositional effects in the underlying substrate atoms (ligand effect) or a reduction in O_{ad} stability due to (repulsive) interactions between neighboring O_{ad} species, has to be clarified in future experiments.

The results presented have important implications for the understanding of PtRu bimetallic catalysts. These are currently considered as very active and CO tolerant catalysts for the electrocatalytic oxidation of H_2 in CO-containing feed gases in low-temperature fuel cells [3], and for the direct methanol oxidation [2]. Based on the results for Pt monolayer island covered Ru(0001) and PtRu(0001) surface alloys, the increased CO tolerance as compared with conventional Pt catalysts can be at least partly explained by the reduced CO adsorption energy on these surfaces, caused by an

electronic modification of the Pt surface atoms due to interaction with neighboring Ru atoms. As a consequence, the desorption rate is increased, and the dynamic equilibrium coverage at operating temperatures of about 330–350 K is reduced, so that the remaining CO adlayer no longer inhibits H_2 adsorption and dissociation. The CO coverage is further reduced by the lower barrier for CO oxidation on the bimetallic PtRu surfaces as compared with the reaction on pure Pt(111). This interpretation is distinctly different from the bifunctional mechanism for CO oxidation on PtRu surfaces suggested earlier as an explanation for the improved CO tolerance of PtRu catalysts [11,12].

Acknowledgements

This work was supported by the EU under contract ERBCHRXCT 930342 in its initial stages. One of us (F.B.d.M.) wants to thank the Alexander von Humboldt-foundation (AvH) for a fellowship, and we also acknowledge financial support from the Conferenza dei Rettori delle Università Italiane (CRUI) and the Deutsche Akademische Auslandsdienst (DAAD) for support via the Vigoni exchange program. Finally, we would like to thank T. Häring for his help in the construction and building up of the TPD system, and J.K. Nørskov (Technical University of Denmark) and H.A. Gasteiger for stimulating discussions.

References

[1] J.H. Sinfelt, Bimetallic Catalysts: Discoveries, Concepts and Applications, Wiley, New York, 1983.
[2] M.P. Hogarth, G.A. Hards, Platinum Metals Rev. 40 (1996) 150.
[3] T.R. Ralph, Platinum Metals Rev. 41 (1997) 102.
[4] S. Aoyoma, European Patent Application EP 0 743 694 A1, 1996.
[5] M. Kahlich, H.A. Gasteiger, R.J. Behm, J. Catal. 171 (1997) 93.
[6] T. Engel, G. Ertl, Adv. Catal. 28 (1979) 1.
[7] J.A. Rodriguez, D.W. Goodman, Surf. Sci. Rep. 1–2 (1991) 223.
[8] H.-I. Lee, G. Praline, J.M. White, Surf. Sci. 91 (1980) 581.
[9] H. Hoffmann, M.D. Weisel, C.F. Peden, Surf. Sci. 253 (1991) 59.
[10] K.L. Kostov, H. Rauscher, D. Menzel, Surf. Sci. 278 (1992) 62.
[11] M. Watanabe, S. Motoo, J. Electroanal. Chem. 60 (1975) 267.
[12] M. Watanabe, S. Motoo, J. Electroanal. Chem. 60 (1975) 275.
[13] H.A. Gasteiger, N. Markovic, P.N. Ross, Jr, E.J. Cairns, J. Phys. Chem. 98 (1994) 617.
[14] M. Scherer, Diploma thesis, Universität Konstanz, 1997.
[15] J.A. Rodriguez, Surf. Sci. Rep. 24 (1996) 223.
[16] B. Hammer, Y. Morikawa, J.K. Nørskov, Phys. Rev. Lett. 76 (1996) 2141.
[17] B. Hammer, J.K. Nørskov, in: R.M. Lambert, G. Pacchioni (Eds.), Chemisorption and Reactivity on Supported Clusters and Thin Films, Kluwer Academic, Dordrecht, 1997, p. 289.
[18] A. Ruban, B. Hammer, P. Stoltze, H.L. Skriver, J.K. Nørskov, J. Mol. Catal. A 115 (1997) 421.
[19] H. Pfnür, P. Feulner, D. Menzel, J. Chem. Phys. 79 (1983) 4613.
[20] E. Kopatzki, S. Günther, W. Nichtl-Pecher, R.J. Behm, Surf. Sci. 284 (1993) 154.
[21] C. Günther, J. Vrijmoeth, R.Q. Hwang, R.J. Behm, Phys. Rev. Lett. 74 (1995) 754.
[22] G. Michalk, W. Moritz, H. Pfnür, D. Menzel, Surf. Sci. 129 (1983) 92.
[23] B. Gleich, M. Ruff, R.J. Behm, Surf. Sci. 386 (1997) 48.
[24] B. Hammer, O.H. Nielsen, J.K. Nørskov, Catal. Lett. 46 (1997) 31.
[25] H.R. Siddiqui, X. Guo, I. Chorkendorf, J.T. Yates, Jr, Surf. Sci. 191 (1987) L813.
[26] A. Szabó, M. Kiskinova, J.T. Yates, Jr, J. Chem. Phys. 90 (1989) 4604.
[27] H. Steininger, S. Lehwald, H. Ibach, Surf. Sci. 123 (1982) 264.
[28] J.C. Bertolini, B. Tardy, M. Abon, J. Billy, P. Delichère, J. Massardier, Surf. Sci. 135 (1983) 117.
[29] R.A. Campbell, J. Rodriguez, D.W. Goodman, Phys. Rev. B 46 (1992) 7077.
[30] R. Wu, Chem. Phys. Lett. 238 (1995) 99.
[31] R. Wu, A.J. Freeman, Phys. Rev. B 52 (1995) 12419.
[32] J. Massardier, B. Tardy, M. Abon, J.C. Bertolini, Surf. Sci. 126 (1983) 154.
[33] J.E. Reutt-Robey, D.J. Doren, Y.J. Chabal, S.B. Christman, J. Chem. Phys. 93 (1990) 9113.
[34] G. Ertl, M. Neumann, K.M. Streit, Surf. Sci. 64 (1977) 393.
[35] T.E. Madey, A. Engelhardt, D. Menzel, Surf. Sci. 48 (1975) 304.
[36] G.E. Thomas, W.H. Weinberg, J. Chem. Phys. 70 (1979) 954.
[37] C.H.F. Peden, D.W. Goodman, J. Chem. Phys. 90 (1986) 1360.
[38] C.H.F. Peden, D.W. Goodman, M.D. Weisel, F.M. Hoffmann, Surf. Sci. 253 (1991) 44.
[39] C. Günther, PhD thesis, Universität München, 1994.
[40] B. Narloch, G. Held, D. Menzel, Surf. Sci. 317 (1994) 131.